*J. Plasma Physics* (2006), *vol.* 72, *part* 6, *pp.* 861–864.  
doi:10.1017/S0022377806005022 Printed in the United Kingdom

# The sidebands instability

MAGDI SHOUCRI[1]

[1]Institut de Recherche d'Hydro-Québec (IREQ), Varennes, Québec J3X 1S1, Canada

(Received 13 August 2005 and accepted 7 December 2005)

**Abstract.** We study numerically the role of mode coupling mechanisms in the generation and growth of sideband modes, during the long time evolution of the nonlinear Landau damping of a large-amplitude wave. The results suggest that a rich variety of wave coupling mechanisms develops during the evolution of the system.

## 1. Introduction

The nonlinear evolution of a large-amplitude wave in a one-dimensional Vlasov plasma is studied with close attention to mode coupling mechanisms as the physical origin of the growth of the sideband modes. The Vlasov equation is solved in phase space by a fractional steps method reported in the literature (Cheng and Knorr 1976; Shoucri and Gagné 1977, 1978; Pohn et al. 2005). In the present work, we allow for longer wavelength modes to be excited by taking the length of the system to be larger than the wavelength of the initially excited wave. We take advantage of the low noise level of the Eulerian Vlasov code by allowing the sidebands to grow from round-off errors.

## 2. The pertinent equations and the results

The pertinent equations are the Vlasov–Poisson system of equations, written in dimensionless form for the electrons in the two-dimensional phase-space $x$–$v$ as

$$\partial_t f + v \cdot \partial_x f - E_x \cdot \partial_v f = 0 \tag{2.1}$$

where $f = f(x, v, t)$ is the electron distribution function and $\partial$ denotes partial derivatives. The spatial dimension $x$ is periodic. Equation (1) is coupled to Poisson's equation:

$$\frac{\partial^2 \varphi}{\partial x^2} = -(1 - n_e) \quad \text{where} \quad n_e = \int_{-\infty}^{\infty} f \, dv \quad \text{and} \quad E_x = -\frac{\partial \varphi}{\partial x} \tag{2.2}$$

Time is normalized to $\omega_p^{-1}$, where $\omega_p$ is the electron plasma frequency, velocity is normalized to the thermal velocity $v_t$, and space is normalized to the Debye length $\lambda_{De} = v_t/\omega_p$. The distribution function is initialized at time $t = 0$:

$$f(x, v, 0) = f_0(v)(1 + \alpha_n \cos(k_n x) + \alpha_{l11} \cos(k_{l11} x) + \alpha_{u13} \cos(k_{u13} x)) \tag{2.3}$$

where $f_0(v)$ is the Maxwellian $f_0(v) = (2\pi)^{-1/2} e^{-v^2/2}$.

The main plasma wave is excited with a perturbation $\alpha_n = 0.18$. We take $L = 80\pi$ for the length of the system and $n = 12$, which leads to a wave number

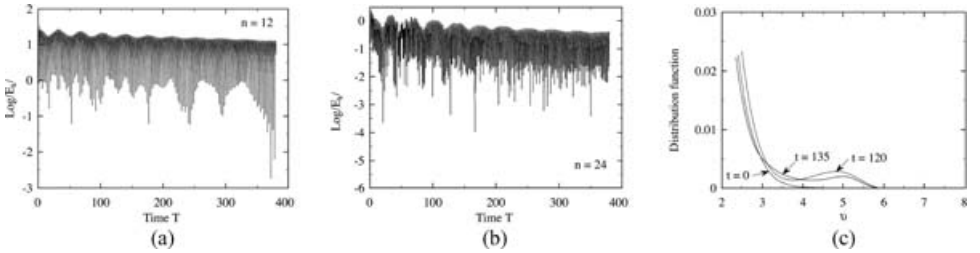


**Figure 1.** Time evolution of the Fourier mode with (a) $n = 12$ and (b) $n = 24$. (c) Tail of the distribution function.

$k_n = 2\pi n/L = 0.3$. The lower sideband with $n = 11$ and a wave number $k_{l11} = 0.275$ and the upper sideband with $n = 13$ and a wave number $k_{u13} = 0.325$ are excited initially with an amplitude of $\alpha_{l11} = 10^{-5}$ and $\alpha_{u13} = 10^{-5}$, respectively, to trigger more rapidly the evolution of the system. If we do not excite them initially, they will grow by themselves from the round-off errors, which will make the evolution of the system very slow since the Vlasov code has a very low noise level.

Details of the Eulerian Vlasov code used to integrate (1) and (2) have been previously reported (Cheng and Knorr 1976; Shoucri 1978, 1979). With $k_n = 0.3$, the linear theory gives, for the real and imaginary parts of the frequency, $\omega_n = 1.1598$ and $\gamma = 0.0126$. The initial kinetic energy of the plasma is 0.5, and the initial electric energy is 0.09. We truncate the distribution function at $|V_{\max}| = 7$. We use 256 points in velocity space, so the recurrence time for the main wave is $T_R = 2\pi/(k_n \Delta v) \approx 381.5\omega_p^{-1}$. We also use 128 points in space, and a time-step $\Delta t = \frac{1}{8}$.

The evolution of the main wave amplitude is shown in Fig. 1(a) on a logarithmic scale. It shows an initial decay with a damping rate of $\gamma = 0.03$ while oscillating with a frequency of $\omega_n = 1.13$. The difference in the values of $\gamma$ and $\omega_n$ with respect to the linear values is due to the initial large-amplitude wave. The bounce frequency of the trapped electrons is $\omega_b = (\alpha_n/2)^{1/2} = 0.3$, resulting in a bounce period of $T_b \approx 21\omega_p^{-1}$. At a time $t$ around $T_b$, the decay of the wave amplitude stops and the amplitude starts growing again (see Fig. 1(a)), then settles to an oscillation that is modulated with a period of approximately $35\omega_p^{-1}$. This modulation corresponds to a similar oscillation in the bump appearing in the tail of the distribution function, shown in Fig. 1(c) at $t = 120\omega_p^{-1}$ and $t = 135\omega_p^{-1}$. The oscillation of the bump settles in the long run to a shape showing a wide bump with a flat minimum around $v \approx 3.8$ and a maximum around $v \approx 5$. The phase velocity of the main wave settles to $1.13/0.3 = 3.76$. This phase velocity is located essentially at the flat minimum of the distribution around $v \approx 3.8$. The bump on the tail corresponds to vortice-like structures appearing in the phase space $x$–$v$, which are traveling at the phase velocity of the main wave (see Figs. 6 and 18 in Shoucri (1978)). We present in Fig. 1(b) the time evolution of the harmonic $k_{2n} = 0.6$. It shows the presence of a frequency of approximately 2.26, i.e. at the harmonic of the frequency of the fundamental mode.

Figs 2(a)–(d) show the lower sidebands with wave numbers of $k_{l11} = 2\pi 11/L = 0.275$, $k_{l10} = 0.25$, $k_{l9} = 0.225$, and $k_{l8} = 0.2$, respectively. The frequencies of the lower sidebands observed numerically are $\omega_{l11} = 1.1$, $\omega_{l10} = 1.068$, $\omega_{l9} = 1.046$, and $\omega_{l8} = 1.00$, respectively. The corresponding phase velocity for the mode $k_{l11}$ is $\omega_{l11}/k_{l11} = 4$, for the mode $k_{l10}$ it is 4.272, and for the mode $k_{l9}$ it is 4.64. These

https://doi.org/10.1017/S0022377806005022 Published online by Cambridge University Press

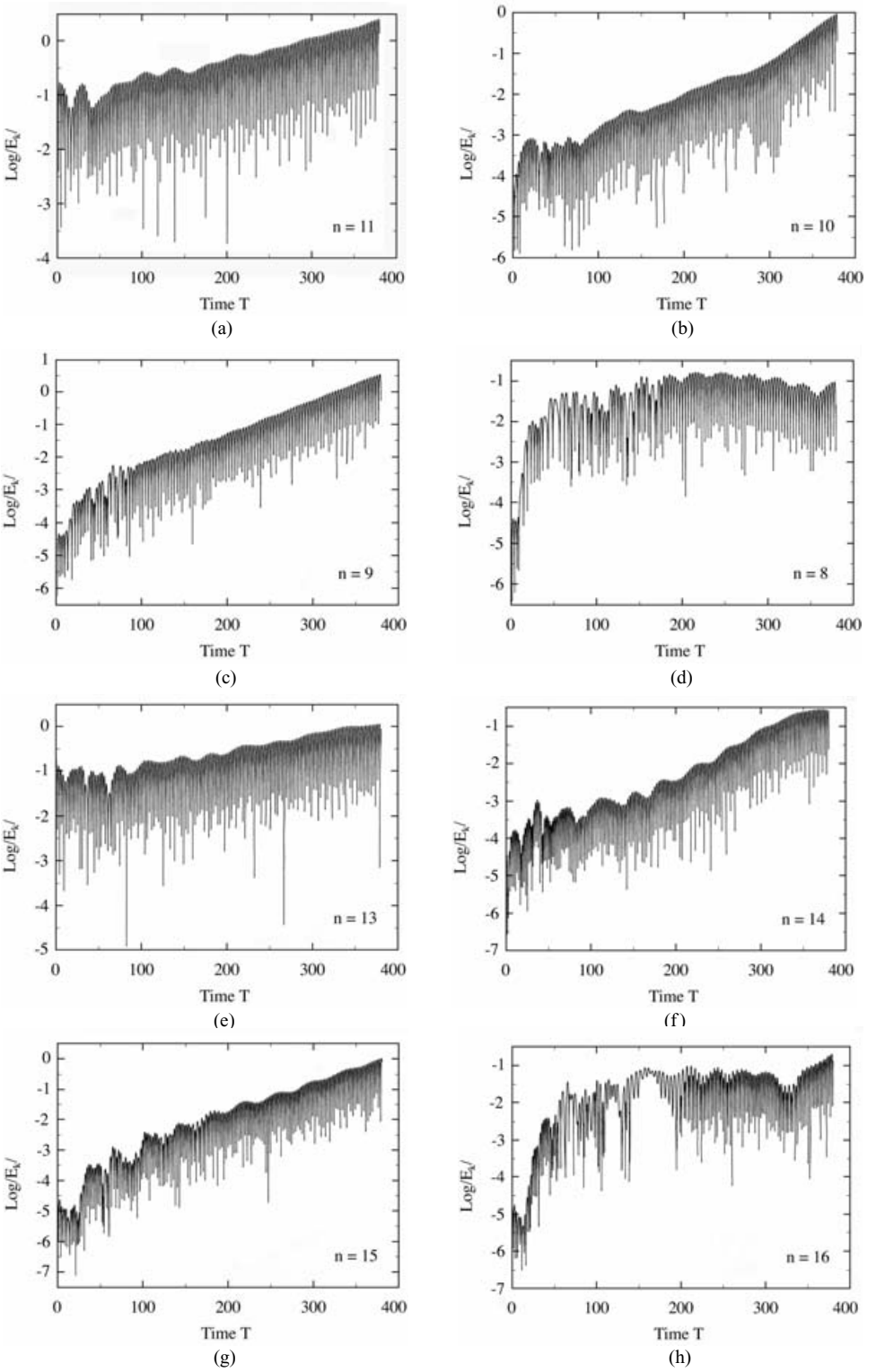


**Figure 2.** Time evolution of the Fourier mode with $n = (11, 10, 9, 8, 13, 14, 15, 16)$ for panels (a)–(h), respectively.

https://doi.org/10.1017/S0022377806005022 Published online by Cambridge University Press

modes have their phase velocities fall on the positive side of the slope of the bump, and show a vigorous growth compared with the other sidebands. The mode $k_{l8}$ has a numerically observed frequency of 1.00, and the corresponding phase velocity is $1.00/0.2 = 5.00$. We see in Fig. 2(d) that this sideband has an evolution different from the previous three: it grows rapidly and then saturates, due to the fact that the phase velocity corresponds to the local flat maximum of the bump in Fig. 1(c) where the slope is zero at $v = 5$.

Figs 2(e)–(h) present the time evolution of the upper sidebands $k_{u13} = 2\pi 13/L = 0.325$, $k_{u14} = 0.35$, $k_{u15} = 0.375$, and $k_{u16} = 0.4$. The frequencies of the first three upper sideband modes are $\omega_{u13} = 1.141$, $\omega_{u14} = 1.196$, and $\omega_{u15} = 1.225$. We note that $\omega_{l11} + \omega_{u13} = 2.241$, $k_{l11} + k_{u13} = 0.6$ and $\omega_{l10} + \omega_{u14} = 2.264$, $k_{l10} + k_{u14} = 0.6$, $\omega_{l9} + \omega_{u15} = 2.271$, $k_{l9} + k_{u15} = 0.6$. We see a good matching of these sidebands with the wave number 0.6 and with the frequency of approximately 2.26 for the harmonic $n = 24$. In Fig. 2(h) towards the end of the evolution, we note a frequency of $\omega_{u16} = 1.27$ for the mode $k_{u16}$. With $\omega_{l8} + \omega_{u16} = 2.27$, $k_{l8} + k_{u16} = 0.6$, this matches with the frequency and wave number of the harmonic $n = 24$. We also note that the upper sideband mode 16 is a harmonic of the lower sideband mode 8, which adds to the complexity of the coupling mechanism. Hence, the combined action of the coupling with the harmonic $k_{2n} = 0.6$ and the positive slope of the distribution acting on the lower sidebands seems to be the mechanism behind the growth. We can also have the coupling of other modes such as $k_{n26} = 0.65$ (harmonic of the upper sideband 13) with $k_{l10}$ and $k_{u16}$ ($k_{l10} + k_{u16} = 0.65$, $\omega_{l10} + \omega_{u16} = 2.338$), or we can have the coupling of the mode $k_{n26} = 0.65$ with $k_{l9}$ and $k_{u17}$ ($k_{l9} + k_{u17} = 0.65$, $\omega_{l9} + \omega_{u17} = 2.37$). Similar couplings can be studied with the mode $k_{n22}$, the harmonic of the mode 11. The excitation of harmonics by wave–wave coupling has been also reported recently by Umeda et al. (2003).

## 3. Conclusions

The appearance of a bump in the tail of the electron distribution function, during the evolution of a large-amplitude wave, is accompanied by the growth of sidebands. A rich variety of wave coupling mechanisms has been studied. For the case treated in Shoucri and Gagné (1978) where the sidebands remained small, the main plasma wave reached indeed a constant amplitude at a phase velocity corresponding to the minimum of a stable bump. In the present work, the evolution of the sidebands has been stopped before they reach the level were they can affect the vortices-like Bernstein–Greene-Kruskal (BGK) structures in phase space. If the sidebands were excited at a higher level, they will reach a level at the end comparable to the main wave, and will then interact with the BGK structures and saturate, while the tail of the electron distribution is distorted to form a flat plateau (Shoucri 1979).

## References

Cheng, C. Z. and Knorr, G. 1976 *J. Comput. Phys.* **22**, 330.
Pohn, E., Shoucri, M. and Kamelander, G. 2005 *Comput. Phys. Comm.* **166**, 81.
Shoucri, M. 1978 *Phys. Fluids* **21**, 1359.
Shoucri, M. 1979 *J. Physique* **40**, C7–575.
Shoucri, M. and Gagné, R. 1977 *J. Comput. Phys.* **24**, 445.
Shoucri, M. and Gagné, R. 1978 *Phys. Fluids* **21**, 1168.
Umeda, T. et al. 2003 *Phys. Plasmas* **10**, 382.